

Potential of Aeroelastic Tailoring to Improve Flutter Stability of Turbomachinery Compressor Blades

C. Reiber, M. Blocher

German Aerospace Center (DLR), Germany,
Bunsenstr a e 10, 37073 G ottingen
Christoph.Reiber@dlr.de, Michael.Blocher@dlr.de

ABSTRACT

To determine the potential of aeroelastic tailoring to improve flutter stability of carbon fiber turbomachinery compressor blades the structural dynamic and aeroelastic behavior of ten different laminate layups were compared. At first an operating point at off-design conditions was identified as flutter critical. Afterwards the dependency between laminate properties and eigenbehavior and between eigenbehavior and aerodynamic stability under these off-design conditions were described.

The results show that for every of the first three natural oscillations certain conditions for the eigenmode and eigenfrequency have to be satisfied to evoke aerodynamically stable behavior. Considering these constraints just one of the investigated laminates is suitable to ensure flutter stability for these certain flow conditions. This very small variety of applicable laminate layups shows the complexity to design aerodynamically stable compressor blades but also the great potential of aeroelastic tailoring to improve the flutter stability of carbon fiber turbomachinery compressor blades.

NOMENCLATURE

k	reduced frequency	φ_ξ	torsional portion
A_{11}	longitudinal stiffness	A_{33}	shear stiffness
W_C	aerodynamic work per cycle	$\vec{f}_{\xi\eta\theta}(t)$	unsteady aerodynamic forces
$\vec{u}_{\xi\eta\theta}(t)$	deformation vector	$E_{kin,max}$	maximum kinetic energy
Λ	aerodynamic damping	$[A]$	A-stiffness-matrix
$[Q_n]$	layer stiffness	t_n	layer thickness
f	oscillation frequency	L_{ref}	reference length
U_{ref}	reference velocity	$\vec{x}_{\xi\eta\theta}(t)$	coordinate vector
φ	deformation portion		

INTRODUCTION

The main objectives during the optimization of turbomachinery compressor blades are a maximization of the aerodynamic efficiency and a minimization of the structural weight. In addition to the optimization objectives different aerodynamic, structural mechanic and aeroelastic constraints have to be considered (Lengyel-Kampmann et al., 2014).

The flutter stability of the rotor depends on the blade vibration in the flow field and the unsteady aerodynamic forces evoked by them. The unsteady pressure on the blade surfaces is influenced by the aerodynamic boundary conditions according to the operating point (Snyder and Burns, 1988) of the investigated system and the motion performed by the blade. Because the operating

conditions are prescribed and part of the optimization, the aeroelastic behavior can only be adjusted by a change of the blade's eigenbehavior.

The usage of fiber reinforced plastic laminates offers the possibility to change the material's direction dependent stiffness by adjusting the laminate layup. Due to the change of the direction dependent stiffness the eigenbehavior of the blade can be adjusted and the geometry is unaffected. Thus the aim of the investigation is to determine how strongly the eigenbehavior and in connection with it the aerodynamic stability can be adjusted by changing the laminate stacking.

INVESTIGATED FAN AND NUMERICAL MODELS

Figure 1 shows the investigated fan, which was developed during the CRISPII and CRISP-multi project at DLR (Lengyel-Kampmann et al., 2014). The main geometrical and design parameters are depicted in table 1. The investigation focuses on two operating points. The first is on the working line at design speed with a pressure ratio of 1.3 and a mach number of 0.68. The second is near the surge line at 70% of the design speed with a pressure ratio of 1.15 and a mach number of 0.29. Beside the second mentioned operating point nine other off-design operating conditions were considered. The operating point at 70% design speed near the surge line was the one with the most critical aeroelastic behavior. Due to the high computational costs a detailed analysis was just carried out for the two mentioned operating conditions.

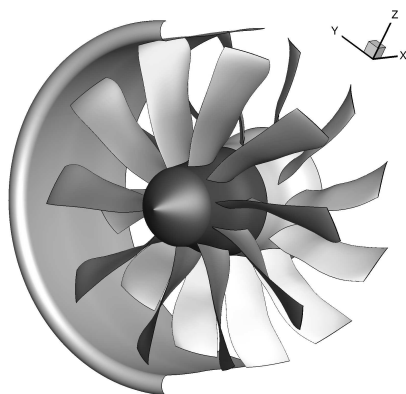


Figure 1: CRISP II

Table 1: geometrical and design parameters

parameter	dimension	rotor 1	rotor 2
number of blades	[]	10,0	12,0
design speed	$[min^{-1}]$	-5044,7	3981,5
blade length	$[mm]$	380,5	343,0
blade width	$[mm]$	145,9	122,8
laminate thickness	$[mm]$	0,5 - 14,2	0,5 -12,4

The structural behavior of the rotors was analysed with the FEM solver MSC Nastran. One blade of each rotor was modeled with approximately 18000 shell elements (CQUAD4). The modal analysis was performed in two steps. First, the model was prestressed by the surface pressure and the rotational forces. Then, the numerical modal analysis was performed, resulting in the eigenmode shapes and the eigenfrequencies of the blade at the operating point.

The aerodynamic analyses were performed with the DLR CFD solver TRACE (Kersken, 2012), which is based on a finite volume method. Assuming cyclic symmetry in the circumferential direction, just one passage of each rotor was modeled by a block structured grid with 800k cells. For steady simulations the Wilcox $k-\omega$ turbulence model and for unsteady linear simulations a frozen viscosity approach with harmonic blade deformation was used.

PROCEDURE AND THEORETICAL CONCEPTS

Flutter stability

The prediction of the flutter stability is based on the determination of the aerodynamic work per cycle W_C , which describes the exchange of energy between blade and flow. Thereby, a positive sign means that energy passes from the flow to the blades vibration leading to an aerodynamically unstable behavior, and a negative sign shows that energy passes from oscillation to flow leading to a damped vibration. The determination of the aerodynamic work is performed on the basis of the energy method by Carta (Carta, 1967). This approach assumes structural dynamic and aerodynamic system as decoupled. Thus, unsteady aerodynamic forces have no influence on the blade's oscillation. Additionally, it is assumed that due to small deformation during the blade's oscillation the unsteady aerodynamic field is composed of a steady part and an unsteady disturbance linear to the vibration amplitude (Kersken, 2012). Via the unsteady aerodynamic pressure on the blade surface the unsteady aerodynamic forces $\vec{f}_{\xi\eta\theta}(t)$ and thereafter via the deformations $\vec{u}_{\xi\eta\theta}(t)$ the aerodynamic work per cycle can be calculated by equation 1. During the flutter analysis, all inter-blade phase angles (Lane, 1956) are considered but just the critical one with the highest aerodynamic work is taken into account. The critical inter-blade phase angle is nearly constant over the different laminates for given operating conditions and eigenmode.

$$W_C = \sum_{\xi\eta\theta} \int_0^T \vec{u}_{\xi\eta\theta}(t) \cdot \vec{f}_{\xi\eta\theta}(t) dt \quad (1)$$

A calculation of the aerodynamic damping Λ (logarithmic decrement) by equation 2 was not performed because according to May (May, 2011) a comparison of the aerodynamic work is more significant due to the normalization of aerodynamic damping by the maximum of kinetic energy $E_{kin,max}$.

$$\Lambda = -\frac{W_C}{2E_{kin,max}} \quad (2)$$

Laminate stiffness

During the modal analysis the structural damping of the material is neglected. Due to the constant geometry the mass matrix is identical for all laminates. Thus, the stiffness is used to characterize the different stackings. Thereby, the laminate layup is symmetric, balanced and composed of eight layers to ensure comparability with the initial laminate. Additionally just layer angles are used which are multiples of 15° and between 0° and 45° to withstand the primary loading (rotation, pressure) of the blade. The laminate stiffness is calculated according to the classical laminate theory (Altenbach et al., 2004) whereby just the longitudinal stiffness A_{11} and the shear stiffness A_{33} component of the A-Matrix $[A]$ are considered because they have the strongest influence on the eigenmodes (bending/torsion). The A-Matrix can be calculated by equation 3 from the layer stiffness $[Q_n]$ in laminate coordinate system and the layer thickness t_n .

$$[A] = \sum_{n=1}^N [Q_n] \cdot t_n \quad (3)$$

Table 2: Investigated laminates and their stiffness values

Nr.	stacking	$A_{11} \left[\frac{kN}{mm} \right]$	$A_{11,Rel} [\%]$	$A_{33} \left[\frac{kN}{mm} \right]$	$A_{33,Rel} [\%]$
1	$[\pm 45^\circ, \pm 45^\circ]_S$	42.603	33.76	32.111	100.00
2	$[\pm 45^\circ, \pm 30^\circ]_S$	60.527	47.96	29.136	90.74
3	$[\pm 30^\circ, \pm 30^\circ]_S$	78.452	62.17	26.162	81.47
4	$[\pm 45^\circ, \pm 15^\circ]_S$	77.420	61.35	23.187	72.21
5	$[\pm 30^\circ, \pm 15^\circ]_S$	95.345	75.55	20.213	62.95
6	$[\pm 15^\circ, \pm 15^\circ]_S$	112.24	88.94	14.264	44.42
7	$[\pm 45^\circ, \pm 0^\circ]_S$	84.401	66.88	20.213	62.95
8	$[\pm 30^\circ, \pm 0^\circ]_S$	102.325	81.08	17.238	53.68
9	$[\pm 15^\circ, \pm 0^\circ]_S$	119.218	94.47	11.289	35.16
10	$[\pm 0^\circ, \pm 0^\circ]_S$	126.199	100.00	8.3148	25.89

Due to the mentioned constraints ten laminates are investigated. Their stackings and stiffness parameters are shown in table 2. All laminates satisfy the requirements for maximum static displacements at the blade tip caused by centrifugal and steady pressure load. The maximum deformations of the blade tips are in a range of less than one millimeter. A change in the material parameters due to temperature impact is not taken into account because the temperature during the rig test is in a range between -10°C and $+30^\circ\text{C}$. The material of the laminates can resist until 120°C .

Reduced frequency and torsional portion

The reduced frequency k and torsional portion φ_ξ of the natural oscillation are important parameters for their aeroelastic behavior (Försching, 1996). The reduced Frequency can be calculated by equation 4 from the oscillation frequency f , a reference length L_{ref} (half chord length) and velocity U_{ref} (averaged convection velocity) of the flow. According to Brouillet (Brouillet, 2001) the limits mentioned in equations 5 and 6 should be respected, regardless if the investigated blade belongs to a compressor or a turbine.

$$k = \frac{2\pi f L_{ref}}{U_{ref}} \quad (4)$$

$$k > 0.3 \quad \text{for bending modes} \quad (5)$$

$$k > 0.7 \quad \text{for torsional modes} \quad (6)$$

The deformation of the blade was analysed by equation 7, thereby coordinates $\vec{x}_{\xi\eta\theta}$ and eigenvector $\vec{u}_{\xi\eta\theta}$ of the FE Nodes are transposed to the blade coordinate system. The blade

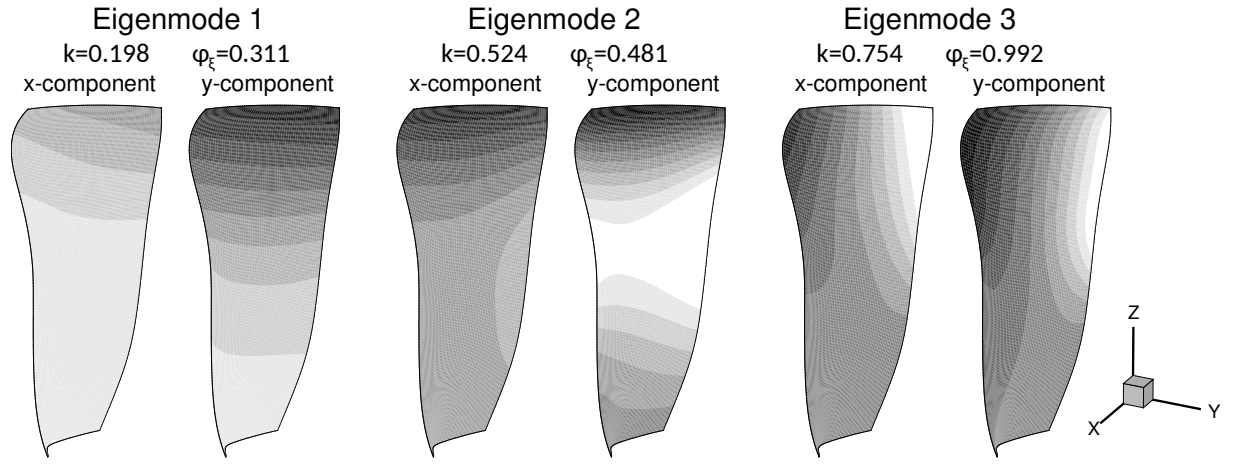


Figure 2: x- and y-component of the eigenmode for the first three natural oscillations

coordinate system is placed in the middle of the chord length at the hub, the ξ -axis points in radial direction, the η -axis in chord direction and the θ -axis is normal two ξ - and η -axis. The blade deformation is normalized to a length of 1.0 and its first component shows the torsional portion φ_ξ of the eigenmode.

$$\vec{\varphi} = \frac{\sum \vec{x}_{\xi\eta\theta} \times \vec{u}_{\xi\eta\theta}}{|\sum \vec{x}_{\xi\eta\theta} \times \vec{u}_{\xi\eta\theta}|} \quad (7)$$

Figure 2 shows x- and y-component of the eigenmode shape over the blade surface for the first three natural oscillations in flow coordinate system and also the values of reduced frequency k and torsional portion φ_ξ for laminate seven under off-design conditions. As depicted in the figure, the blade performs for first and second natural oscillation primary bending and for third natural oscillation primary torsional motions. Nevertheless, the values of torsional portion show that no clear separation between bending and torsional eigenmode is possible. Thus, according to the limit of 0.7 for reduced frequency the first three eigenmodes have to be respected for flutter analysis.

RESULTS

The presentation of the results is splitted in three parts. At first the aerodynamic damping of two different operating points is compared. The comparison shows that aerodynamic unstable behavior occurs for the investigated fan just under off-design conditions. The second and third part of the subsection focuses on modal analysis and flutter analysis results under these off design conditions. According to the results different requirements for the laminates were derived to ensure aerodynamic stability in the first three eigenmodes.

Aerodynamic stability under different operating conditions

The aerodynamic work is plotted over the reduced frequency for an operating point with design conditions in figure 3 and for an operating point at part rotational speed near the surge line in figure 4. The graphics show that under design conditions all laminates behave aerodynamically stable and under off-design conditions a major part of the laminates behave aerodynamically unstable especially for the first and third eigenmode.

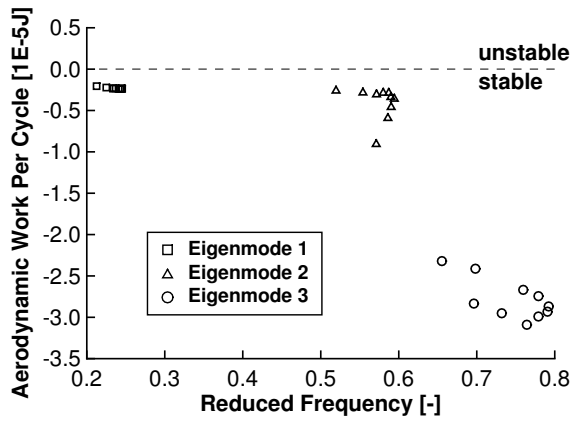


Figure 3: Aerodynamic work over reduced frequency for the first three eigenmodes at design operating conditions

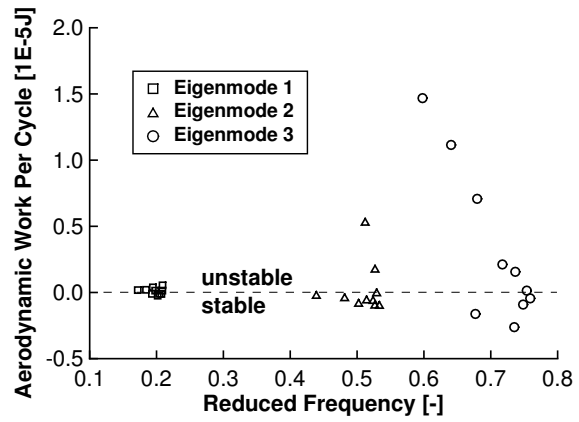


Figure 4: Aerodynamic work over reduced frequency for the first three eigenmodes at off-design operating conditions

For the first eigenmode the laminates show under design conditions nearly constant negative aerodynamic work over reduced frequency. In contrast, the major portion of the laminates are aerodynamically unstable under off-design conditions and the scatter of aerodynamic work over reduced frequency is higher than under design conditions. The second natural oscillation is less critical than the first but for both operating points the aerodynamic work of two laminates have a high difference to the other. Under design conditions these laminates are more stable, under off-design conditions less stable, leading to aerodynamic instability. The aerodynamic behavior for the third natural oscillation shows high differences for both operating points, whereby under design conditions the laminates have the lowest and under off-design conditions the highest aerodynamic work. According to the presented results the operating point at off-design conditions is identified as flutter critical and used for detailed investigations.

Modal Analysis

First natural oscillation

Reduced frequency over longitudinal stiffness is presented in figure 5. The value of the reduced frequency is increasing for laminates with higher longitudinal stiffness but the slope of the curve is decreasing. The values range between 0.17 and 0.21 thus no laminate reaches the limit mentioned in equation 5 for bending eigenmodes.

The torsional component of the eigenmode over the shear stiffness is shown in figure 6. As depicted in the figure, the torsional part of the blade motion is decreasing for laminates with high shear stiffness. The torsional portion is between 0.1 and 0.5 which illustrates that all laminates have a high bending portion in the first natural oscillation and a strong influence of laminate stiffness on the eigenvector.

The eigenfrequency of a natural oscillation is increasing if the stiffness in the direction of the eigenmode is increasing. Thus, an increasing in stiffness against a specified motion leads to a decrease of the motions proportion in the eigenmode. Additionally, laminates with a high longitudinal stiffness have a high proportion of 0° plies and thus a lower proportion of 45° plies leading to lower shear stiffness. So the laminates with highest shear stiffness have the lowest longitudinal stiffness and so high resistance against torsional and low resistance against bending motion resulting in an oscillation with low torsional portion (high bending portion) and a

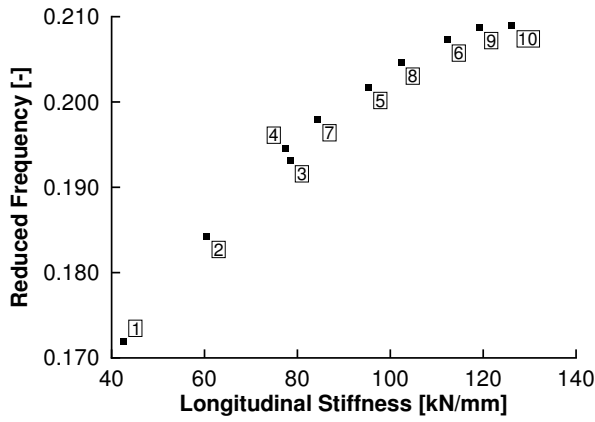


Figure 5: **Reduced frequency over longitudinal stiffness for the first natural oscillation**

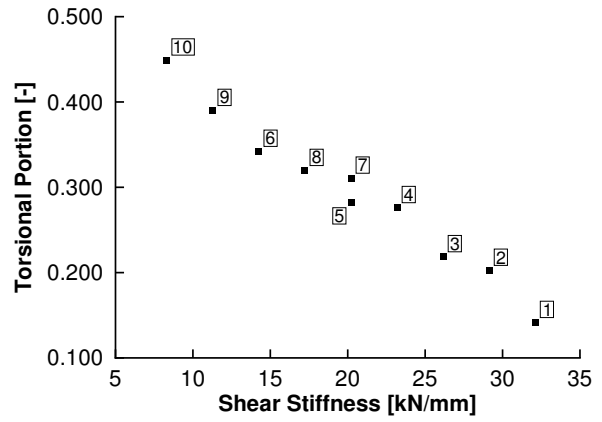


Figure 6: **Torsional portion of the eigenmode over shear stiffness for the first natural oscillation**

low reduced frequency. An increase in longitudinal stiffness leads to an increase in reduced frequency and torsional portion (less bending portion) because the resistance against bending motions is getting higher. Additionally, the shear stiffness and resistance against torsional motions decreases leading to a smaller increase of reduced frequency for laminates with higher longitudinal stiffness shown in figure 5.

Second natural oscillation

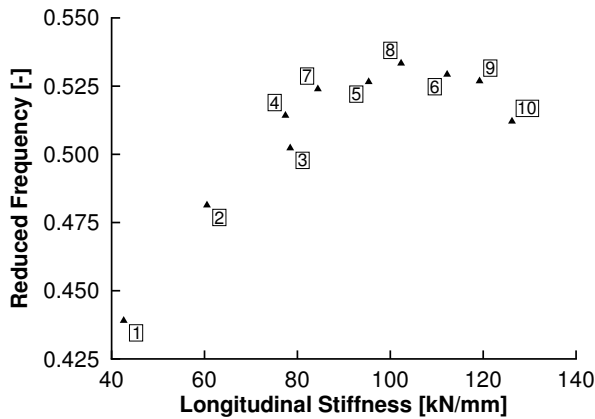


Figure 7: **Reduced frequency over longitudinal stiffness for the second natural oscillation**

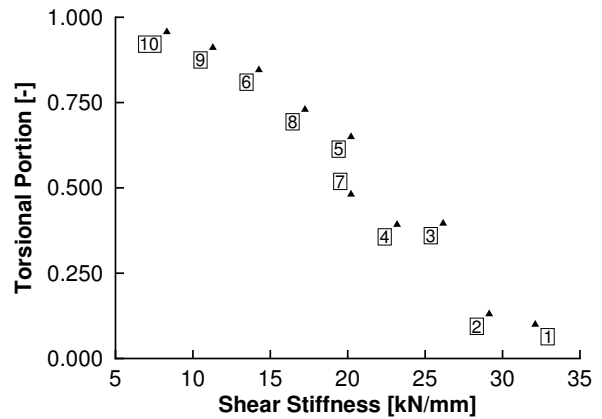


Figure 8: **Torsional portion of the eigenmode over shear stiffness for the second natural oscillation**

Figure 7 illustrates reduced frequency plotted over the longitudinal stiffness. Similar to the first natural oscillation, the reduced frequency is increasing for laminates with higher stiffness in longitudinal direction, but the maximum reduced frequency is shifted slightly away from laminates with maximum longitudinal stiffness. The values range between 0.425 and 0.55 thus according to equations 5 and 6 the constraint for bending modes (0.3) is satisfied and for torsional modes (0.7) unsatisfied.

Figure 8 shows the torsional component of the eigenvector over the shear stiffness. Similar to the first natural oscillation a higher shear stiffness leads to a lower torsional portion in the eigenmode. The reason for this course is the effect described for the first natural oscillation. The major difference is that the torsional proportion ranges from 0.0 to 1.0. Thus, the blade motion for laminates with high shear stiffness is a bending mode and for laminates with lower shear stiffness a torsional mode. In contrast to the first natural oscillation, the high proportion of torsional motion leads for laminates with high longitudinal stiffness to a decrease in reduced frequency. Laminates with slightly increased shear stiffness show the highest reduced frequency because the resistance against torsional motions leads to lower torsional proportion and in connection with the higher longitudinal stiffness to the maximum of reduced frequency.

Third natural oscillation

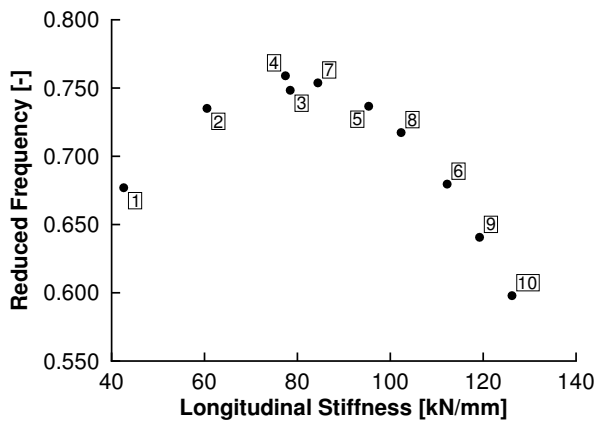


Figure 9: **Reduced frequency over longitudinal stiffness for the third natural oscillation**

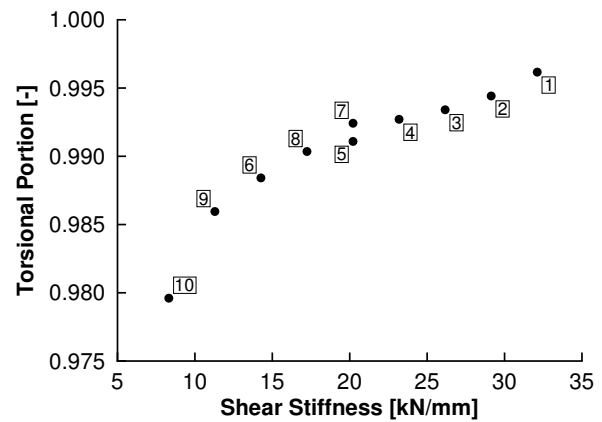


Figure 10: **Torsional portion of the eigenmode over shear stiffness for the third natural oscillation**

A plot of the reduced frequency over the longitudinal stiffness is presented in figure 9. The graphic shows that the local maximum is shifted to laminates with lower longitudinal stiffness in comparison with the first two natural oscillations. The values range between 0.55 and 0.8 thus the limit for bending modes (0.3) is reached for every laminate and the constraint for torsional modes (0.7) is also partly satisfied.

Figure 10 illustrates the torsional component of the eigenmode over the shear stiffness. In contrast to the first and second natural oscillation the torsional portion of the eigenmode is increasing for laminates with higher shear stiffness which is contradictory to the effect described before. The difference to the first two natural oscillations is that the torsional portion ranges just from 0.975 to 1.0. So all laminates show a torsional motion and the influence of the shear stiffness on the eigenmode is almost negligible.

Flutter Analysis

First natural oscillation

Aerodynamic work is plotted against reduced frequency in figure 11 and against torsional portion in figure 12. The numbering of the symbols is the same as the numbering of the laminates in table 3. In both figures no direct parametric influence is apparent because the com-

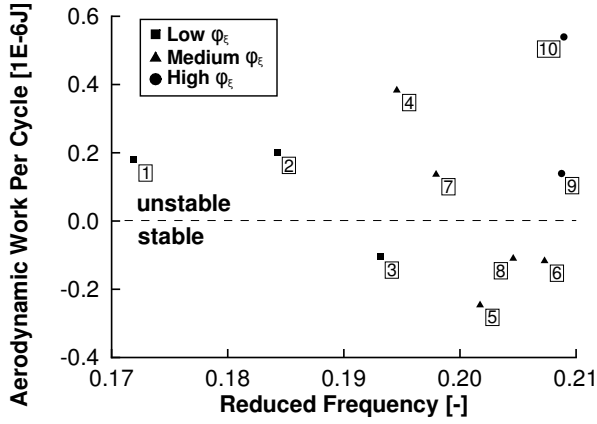


Figure 11: Aerodynamic work per cycle over reduced frequency for the first natural oscillation at critical Operating Point

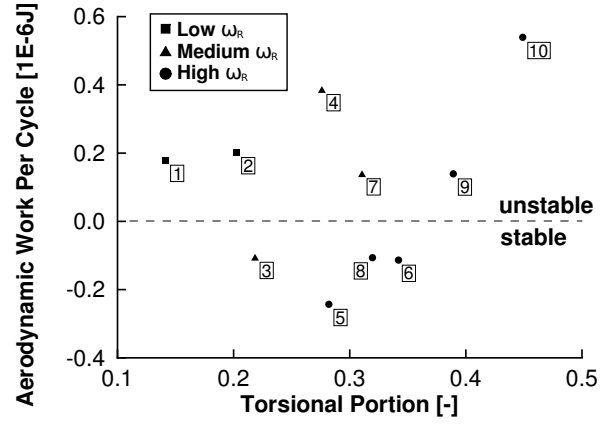


Figure 12: Aerodynamic work per cycle over torsional portion for the first natural oscillation at critical Operating Point

bination of reduced frequency and torsional portion is decisive. To show the influence of the eigenmode in figure 11 laminates with low ($0.10 \leq \varphi_{\xi} \leq 0.25$), medium ($0.25 \leq \varphi_{\xi} \leq 0.35$) and high ($0.35 \leq \varphi_{\xi} \leq 0.50$) torsional portion are plotted with different symbols. Additionally laminates with low ($0.17 \leq k \leq 0.19$), medium ($0.19 \leq k \leq 0.20$) and high ($0.20 \leq k \leq 0.21$) reduced frequencies are marked with different symbols in figure 12.

The symbols show in both graphics that laminates with a low torsional portion are stable ($0.10 \leq \varphi_{\xi} \leq 0.25$) if their reduced frequency is medium ($0.19 \leq k \leq 0.20$) and unstable if their reduced frequency is low ($0.17 \leq k \leq 0.19$). Additionally laminates with medium torsional portion ($0.25 \leq \varphi_{\xi} \leq 0.35$) are stable if their reduced frequency is high ($0.20 \leq k \leq 0.21$) and unstable if their reduced frequency is medium ($0.19 \leq k \leq 0.20$). Laminates with high torsional portion ($0.35 \leq \varphi_{\xi} \leq 0.50$) always show unstable behavior.

The results show in accordance to equations 5 and 6 that an increase in reduced frequency leads to an increase in aerodynamic stability and an increase in torsional portion leads to a decrease in aerodynamic stability. Furthermore, the laminate with stable behavior at low torsional portion (bending mode) shows a reduced frequency higher than 0.19 which indicates that the limit for bending modes (0.3) has to be adjusted for the investigated turbomachinery compressor blades.

Additionally, in connection with the results of the modal analysis, constraints for aerodynamically stable behavior can be derived. Laminates are stable if their reduced frequency is high and torsional portion is medium (e.g. Laminate 8) or if their reduced frequency is medium and torsional portion is low (e.g. Laminate 3). In contrast laminates are unstable if their reduced frequency is high and also their torsional portion is high (e.g. Laminate 10) or if their reduced frequency is medium and torsional portion is medium to high (e.g. Laminate 4). Relating to the modal analysis results laminates with high longitudinal stiffness and moderate shear stiffness (e.g. Laminate 8) or moderate longitudinal and high shear stiffness (e.g. Laminate 3) are necessary for aerodynamically stable behavior. Laminates with high longitudinal stiffness and low shear stiffness (e.g. Laminate 10) or medium longitudinal and medium shear stiffness (e.g. Laminate 4) show unstable aerodynamic behavior.

Second natural oscillation

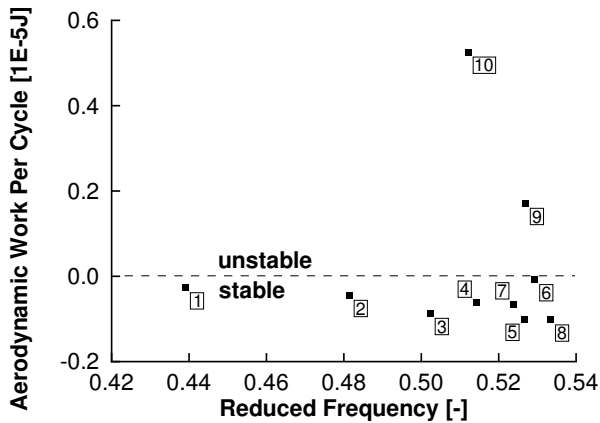


Figure 13: **Aerodynamic work per cycle over reduced frequency for the second natural oscillation at critical Operating Point**

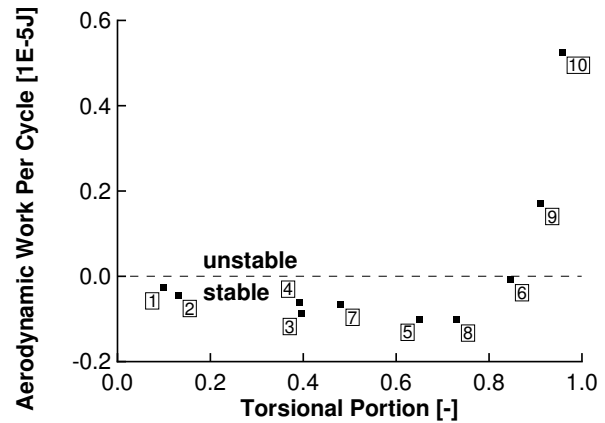


Figure 14: **Aerodynamic work per cycle over torsional portion for the second natural oscillation at critical Operating Point**

Aerodynamic work is plotted against torsional portion in figure 14 and against reduced frequency in figure 13. The plot over the torsional portion shows that the eigenmode is the decisive parameter for the second natural oscillation because aerodynamic work is strongly increasing if the torsional portion is higher than 0.8.

According to the theory and similar to the first natural oscillation laminates are more unstable if their torsional portion is higher. Relating to the constraints for reduced frequency the laminates with lower torsional portion show in comparison to the unstable laminates a nearly constant aeroelastic behavior.

In connection with the modal analysis results laminates with low shear stiffness show a high torsional portion and a reduced frequency slightly lower than the maximum. According to the results, the second natural oscillation is stable if the blades motion is not a torsional eigenmode. Thus, a moderate to high shear stiffness is necessary for aerodynamic stable behavior.

Third natural oscillation

Aerodynamic work is plotted against reduced frequency in figure 15 and against torsional portion in figure 16. As depicted in the figures aerodynamic work is decreasing for higher reduced frequencies and torsional portions. According to modal analysis the torsional portion is increasing for laminates with higher shear stiffness for the third natural oscillation but the maximum reduced frequency is slightly shifted to lower longitudinal stiffness.

Overall result

In table 3 the laminates showing aerodynamically stable behavior are marked by an x and additionally the relative longitudinal and shear stiffnesses to compare the results with the constraints mentioned before. The marked boxes show the complexity to design an aerodynamically stable laminate for the investigated turbomachinery compressor. Just laminate three satisfies all constraints for aerodynamically stable behavior.

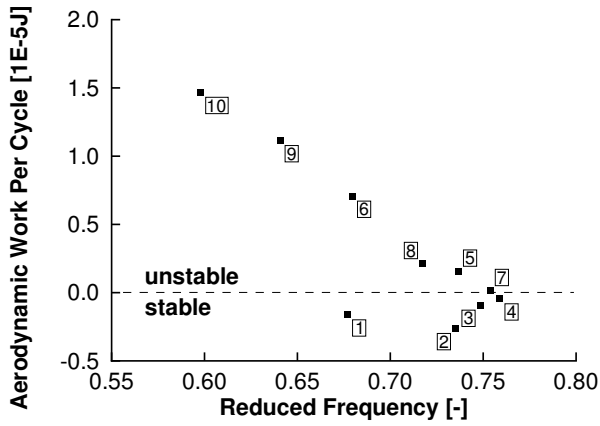


Figure 15: Aerodynamic work per cycle over reduced frequency for the third natural oscillation at critical OperatingPoint

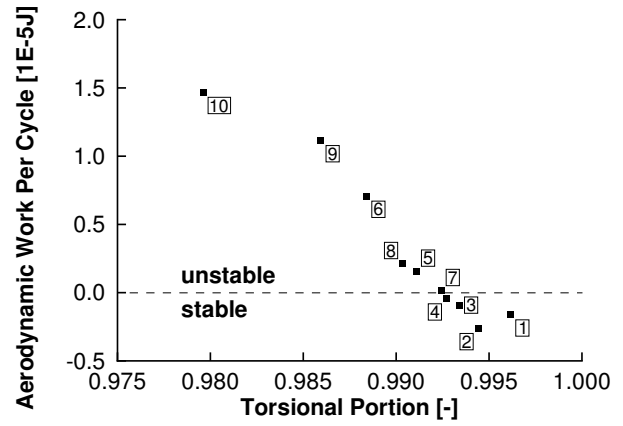


Figure 16: Aerodynamic work per cycle over torsional portion for the third natural oscillation at critical Operating Point

Table 3: Laminates, stiffness values and aerodynamic stability (x = stable)

Nr.	1	2	3	4	5	6	7	8	9	10
A_{11} [%]	33.76	47.96	62.17	61.35	75.55	88.94	66.88	81.08	94.47	100.00
A_{33} [%]	100.00	90.74	81.47	72.21	62.95	44.42	62.95	53.68	35.16	25.89
Mode 1			x		x	x		x		
Mode 2	x	x	x	x	x	x	x	x		
Mode 3	x	x	x	x						

CONCLUSIONS

Three different investigations were used to determine the influence of laminate parameters on the aerodynamic stability of a fan. First up, a comparison between two operating points was used to identify the off-design conditions as flutter critical and subsequently a modal and a flutter analysis were performed for these operating conditions. The results show that the knowledge of flutter critical areas in the compressor map is necessary for a successful analysis.

Furthermore, the results show that the structural and aeroelastic behavior can be influenced strongly by the stacking of the applied laminate. Especially for the modal analysis strong dependency between longitudinal stiffness and reduced frequency and between torsional portion and shear stiffness was presented and described.

The flutter analysis shows in accordance to the theory that the combination of reduced frequency and torsional portion of the eigenmode is decisive for the aerodynamic stability. In connection with the modal analysis different constraints for laminate properties and stacking which are necessary for flutter stability were mentioned.

Additionally it was shown that just one of the ten investigated laminates show aerodynamic stable behavior for the first three natural oscillations in the critical operating point. Overall the

results show the complex dependencies between laminate stacking and aeroelastic behavior but also the great potential of aeroelastic tailoring to improve the flutter stability of carbon fiber turbomachinery compressor blades.

REFERENCES

- Altenbach, H., Altenbach, J., and Kissing, W. (2004). *Mechanics of Composite Structural Elements*. Springer.
- Brouillet, B. (2001). *Zeitgenaue dreidimensionale Simulation des Flatterns in Turbomaschinen durch numerische Lösung der Navier-Stokes-Gleichungen*. PhD thesis, Technical University Aachen.
- Carta, F. O. (1967). *Coupled Blade-Disk-Shroud Flutter Instabilities in Turbojet Engine Rotors*. J ENG GAS TURB POWER, 89:419–426.
- Försching, H. (1996). *A parametric study of the flutter stability characteristics of turbomachine cascades*. ASME. Turbo Expo: Power for Land, Sea, and Air, Vol. 5: *Manufacturing Materials and Metallurgy; Ceramics; Structures and Dynamics; Controls, Diagnostics and Instrumentation*(96-GT-260).
- Kersken, H.-P. (2012). *Time-linearized and time-accurate 3d rans methods for aeroelastic analysis in turbomachinery*. J Turbomach, Vol. 134:051024.
- Lane, F. (1956). *System mode shapes in the flutter of compressor blade rows*. AIAA Journal of the Aeronautical Sciences, 23:54–66.
- Lengyel-Kampmann, T., Voß, C., Nicke, E., Rüd, K.-P., and Schaber, R. (2014). *Generalized optimization of counter-rotating and single-rotating fans*. ASME. Turbo Expo: Power for Land, Sea, and Air, Volume 1A: Aircraft Engine; Fans and Blowers, 134:GT2014–26008.
- May, M. (2011). *Linearized Flutter Investigations of Mistuned Turbomachinery Blading*. PhD thesis, DLR Göttingen.
- Snyder, L. and Burns, D. (1988). *Forced vibration and flutter design methodology*. In AGARD Manual on Aeroelasticity in Axial-Flow Turbomachines, volume 2: *Structural Dynamics and Aeroelasticity*, pages 22–1 – 22–28. Platzer M. F. and Carta F.O.